NANO · MICRO small
www.small-journal.com

Electrosynthesis of Ionic Covalent Organic Frameworks for Charge-Selective Separation of Molecules

Xingyuan Wang, Jingying Yang, Xiansong Shi, Zhe Zhang, Congcong Yin, and Yong Wang**

Covalent organic frameworks (COFs) have emerged as potent material platforms for engineering advanced membranes to tackle challenging separation demands. However, the synthesis of COF membranes is currently hampered by suboptimal productivity and harsh synthesis conditions, especially for ionic COFs with perdurable charges. Herein, ionic COFs with charged nanochannels are electrically synthesized on conductive supports to rapidly construct composite membranes for charge-selective separations of small molecules. The intrinsic charging nature and strong charge intensity of ionic COFs are demonstrated to collectively dominate the membrane growth. Spontaneous repairing to diminish defects under the applied electric field is observed, in favor of generating well-grown COF membranes. Altering electrosynthetic conditions realizes the precise control over the membrane thickness and thus the separation ability. Electrically synthesized ionic COF membranes exhibit remarkable molecular separation performances due to their relatively ordered and charged nanochannels. With these charge-selective pathways, the membranes enable the efficient sieving of charged and neutral molecules with analogous structures. This study reveals an electrical route to synthesizing COF thin films, and showcases the great potential of ionic nanochannels in precise separation based on charge selectivity.

1. Introduction

Covalent organic frameworks (COFs), a versatile kind of crystalline porous polymers organized by predictably stitching monomers through covalent bonds, have aroused escalating interest since the pioneering report by Yaghi et al.[1] Featuring permanent porosity, well-defined pores, and structural diversity, COFs have been extensively studied for a variety of applications related to energy and environment.[2] With the advantages of their ordered, size-tunable pores and devisable pore-wall environments, COFs also emerge as reliable materials to construct membrane platforms for challenging separation needs.[3]

X. Wang, J. Yang, X. Shi, Z. Zhang, C. Yin, Y. Wang
State Key Laboratory of Materials-Oriented Chemical Engineering
College of Chemical Engineering
Nanjing Tech University
Nanjing 211816, P. R. China
E-mail: xsshi@njtech.edu.cn; yongwang@njtech.edu.cn

The ORCID identification number(s) for the author(s) of this article can be found under https://doi.org/10.1002/smll.202107108.

DOI: 10.1002/smll.202107108

Up to now, an array of effective strategies, such as interfacial polymerization,[4] solvothermal growth,[5] and nanosheet assembly,[6] have been progressively developed to produce homogeneous COF-based membranes for molecular and ionic separations. Among these currently available methods, COF selective layers are either directly synthesized on porous supports or crystallized at the interface followed by transferring onto supports. Thus, the accessibility to COF membranes is substantially contingent upon the strict and rational design of the substrate properties, including pore sizes, solvent resistance, and surface functionality.[7] Moreover, due to the lack of feasible and high-efficiency methods, improving the productivity of COF membranes still faces a major challenge. Being challenged by these obstacles, it is imperative to explore innovative synthesis strategies enabling the facile and highly efficient production of COF membranes on various supports.

Electrosynthesis has been widely employed as a viable approach to generating thin films on a wide range of conductive substrates.[8] It stands out among the existing film fabrication techniques mainly due to its highlighted merits including high productivity and mild operation conditions.[9] Also importantly, precise control over the film growth can be readily exerted by adjusting the electrical parameters, resulting in well-regulated film structures.[10] The implementation of growing diverse films, comprised of metal–organic frameworks (MOFs),[11] conjugated microporous polymers (CMPs),[12] hydrogen-bonded organic frameworks (HOFs),[13], etc.,[14] manifestly illustrates the prominent feasibility and universality of this methodology. Electrochemical polymerization and electrophoretic deposition are the two main approaches to the preparation of separation membranes via electrosynthesis. Electrochemical polymerization relies on the electrically triggered reactions on electrodes, which start from molecular building blocks.[15] For example, Lai et al. reported the electropolymerization strategy to fabricate CMP membranes for high-precision separations.[16] Additionally, a current-driven method has been proposed for fabricating MOF membranes on inorganic and organic substrates, with significantly shortened synthesis durations of several minutes.[17] Alternatively, the electrophoretic deposition focuses on the

directional migration and assembly of charged nanoparticles on the electrodes by applying an electric field to their dispersions.[18] This strategy can in principle generate continuous films on arbitrary conductive supports. Taking ZIF-8 as an example, various supports regardless of the surface porosity have been used to grow the corresponding membranes through this method.[19]

Although the applicability of electrosynthesis in universally producing separation membranes has been vastly demonstrated, its accessibility to COF membranes is rarely explored, probably due to the following obstacles. On the one hand, the electrochemical synthesis of microporous organic membranes, especially CMPs, largely relies on the polymerization of precursors with electroactive structures, such as carbazole, triphenylamine, and thiophene.[20] The absence of these specific groups in COF monomers primarily encumbers the electrochemical co-polymerization of the monomer pairs. On the other hand, COF nuclei are usually spontaneously generated in the bulk solution upon the mixing of monomers due to the high reactivity of monomers,[21] posing a considerable challenge for electrochemical synthesis. Therefore, the electrosynthesis of COF films is mostly focused on the electrodeposition of COF dispersions obtained by exfoliating solvent-thermally synthesized bulk counterparts.[8] Due to the structural rigidity and suboptimal exfoliation efficiency, the prepared dispersions are usually composed of COF particles with sizes ranging from several tens of nanometers to a few microns. The deposition of such large-sized COF dispersions could result in films with defective interparticle gaps. In addition, the charge neutrality of most developed COFs impedes their migration under electric stimulations, and high electric field intensities (up to 900 V cm^{-1}) are usually involved.[22] The designed synthesis of ionic COFs with abundant charge sites on their skeletons has recently brought light to the low-voltage preparation of COF films.[23] Nevertheless, the aforesaid issue of loosely stacked topographies derived from the dispersion deposition method stands unsolved. It has been reported that by employing ionic precursors, the current-driven self-repairing can be implemented for the in situ synthesis of compact MOF membranes.[17] Inspired by this mechanism, we speculate that applying ionic molecules as the monomer to prepare COF membranes through electrosynthesis could possibly ensure the membrane integrity for separation applications.[17,21,24] Thus-synthesized membranes could take the intrinsic advantages of COFs as well. More importantly, the ionic building blocks inherently generate charge-enriched mass transfer routes, thus benefiting the charge-enhanced selectivity.

In this work, we have developed a novel electrosynthesis method empowering the rapid generation of ionic COF membranes for charge-selective molecular sieving. The membrane formation is jointly controlled by the electric-driven migration and the directional assembly of ionic monomers and COF nuclei. Spontaneous repairing through reversible Schiff-base reactions and region-selective deposition is implemented to guarantee the membrane integrity. By applying this strategy, ionic COF membranes can be readily produced within 3 h, which further render a remarkably high water permeance of ≈344.6 L m^{-2} h^{-1} bar^{-1} and >90% rejection to small molecules. We also illustrate that the charge-selective nanochannels in the resulting membranes can precisely discriminate charged and neutral molecules, showing great potential in tackling intractable separation needs.

2. Results and Discussion

2.1. Electrosynthesis of TpEB Films

In this work, TpEB, which is synthesized via the condensation of 1,3,5-triformylphloroglucinol (Tp) and ethidium bromide (EB), is selected as the representative ionic COF for investigation. Electrosynthesis of TpEB films was first performed on nonporous indium-doped tin oxide (ITO) conductive glasses using acetic acid (AA) as the catalyst under the electric field intensity of 50 V cm^{-1}. As schematically illustrated in **Figure 1**a and Figure S1 (Supporting Information), the electrical growth of TpEB films was carried out in a homemade synthesis device where the condensation of the monomer pairs rapidly occurs. After 3 h of synthesis, a uniform light brown covering appears exclusively on the surface of the cathode ITO support, while the anode remains unchanged (Figure 1b; Figure S2, Supporting Information). The color of the formed covering matches well with TpEB powders,[25] indicating the generation of TpEB. The unilateral growth presented here not only substantiates the condensation reaction but also identifies the electrically governed migration of charged monomers and crystal nuclei from cathode to anode. The targeted movement is consistent with the motion law of charged objects in electric field.[18a] The field-emission scanning electron microscopy (SEM) images shown in Figure 1c–d further reveal a continuous and defect-free layer with a thickness of ≈340 nm, visually confirming the successful formation of TpEB films.

Chemical composition and structure of the TpEB powders produced by electrosynthesis (TpEB-ES) and solvothermal synthesis (TpEB-ST) were characterized for comparison. According to the Fourier transform infrared (FT-IR) spectra in **Figure 2**a and Figure S3a (Supporting Information), the absence of C=O (1630 cm^{-1}) and $-NH_2$ (3400–3100 cm^{-1}) characteristic peaks, which belong to Tp and EB respectively, indicates the consumption of the monomer pairs. Also, both of the powders exhibit new characteristic peaks of C=C (1580 cm^{-1}) and C−N (1250 cm^{-1}), confirming the formation of TpEB under these two conditions.[26] The formation of TpEB can also be clarified by the ^{13}C solid-state nuclear magnetic resonance (NMR), with signals from carbon atoms in the C=C and C−N groups at ≈128, ≈165, and ≈148 ppm (Figure S3b, Supporting Information). We subsequently studied the structural regularity of the TpEB powders. The X-ray diffraction (XRD) pattern of TpEB-ST powder exhibits a sharp diffraction peak at ≈3.6° and a wide diffraction peak at ≈27° (Figure S3c, Supporting Information), which can be assigned to the (100) and (001) planes, respectively, hinting at a high crystallinity.[27] For TpEB-ES powder, the diffraction peak appears at ≈3.8°, but with reduced intensity (Figure 2b). Catalysts typically play a vital role in crystalizing building blocks into COF materials.[28] With this in mind, we optimized the catalysis conditions in order to obtain high-crystallinity TpEB-ES powders during electrosynthesis. It is observed in

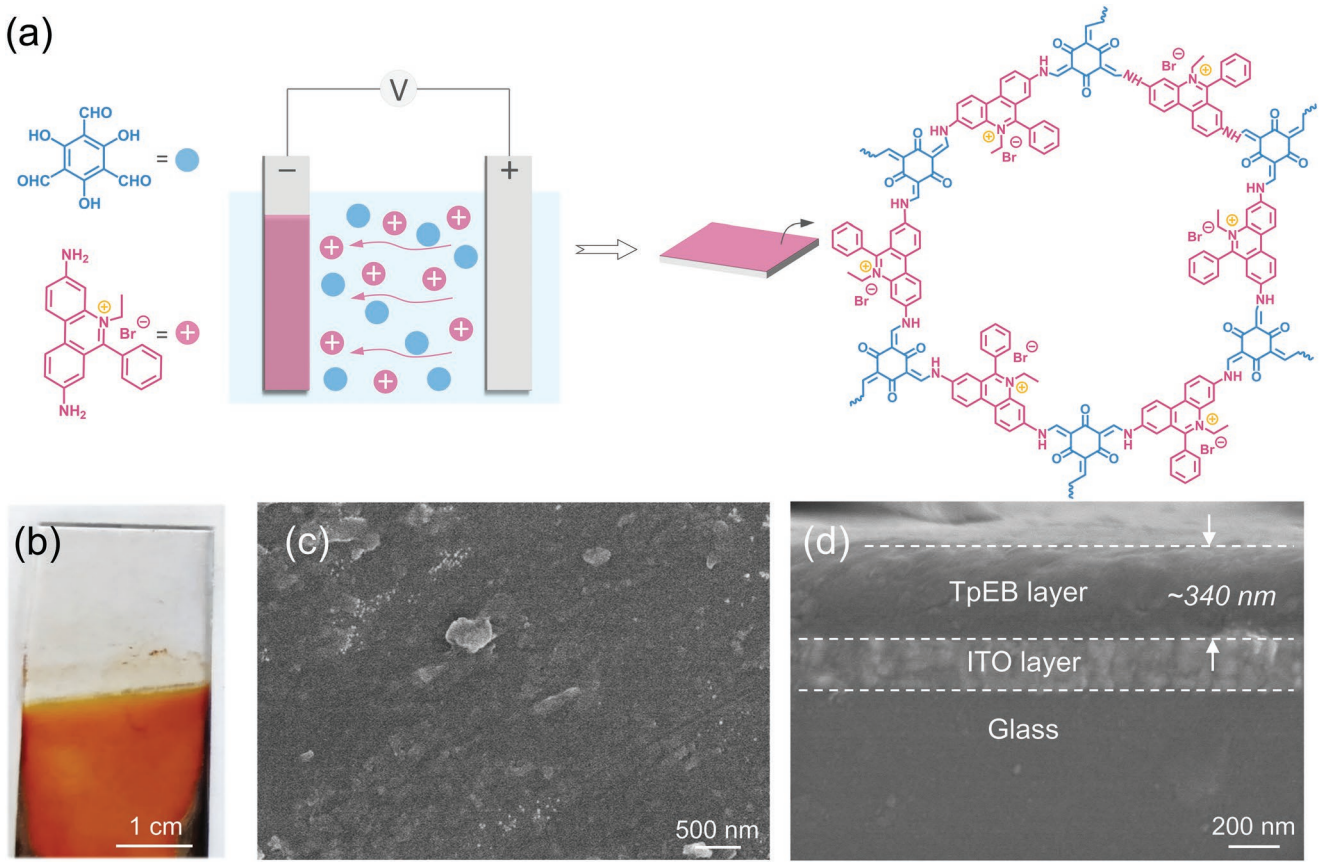

Figure 1. Electrosynthesis of TpEB films on ITO supports. a) Schematic illustration of the synthesis process. b) Digital image, c) surface, and d) cross-sectional SEM images of the TpEB-grown ITO support.

Figure 2b that the raise in AA amount largely improves the crystallinity, as confirmed by the intensive diffraction peak at ≈3.8°. Surprisingly, the powder crystallinity is further enhanced when using scandium(III) triflate, i.e., $Sc(OTf)_3$, instead of AA as the catalyst. These results validate an insightful influence of catalysts on the crystallization of TpEB by electrosynthesis. N_2 adsorption–desorption isotherms show that the Brunauer–Emmett–Teller (BET) surface area of the TpEB-ST powder is 239.3 $m^2\ g^{-1}$, whereas the value of the AA-catalyzed TpEB-ES powder decreases obviously (Figure S3d–e, Supporting Information). This can be mostly attributed to the compromised crystallinity of TpEB-ES resulting from the extremely mild conditions of this electrosynthesis strategy. Different from conventional COF materials, rigorous conditions are of vital necessity for the synthesis of highly crystalline ionic COFs, potentially due to the electrostatic interactions between the adjacent ionic COF layers.[29] This accordingly rationalizes the moderate crystallinity and surface area of TpEB-ES powder. Interestingly, the

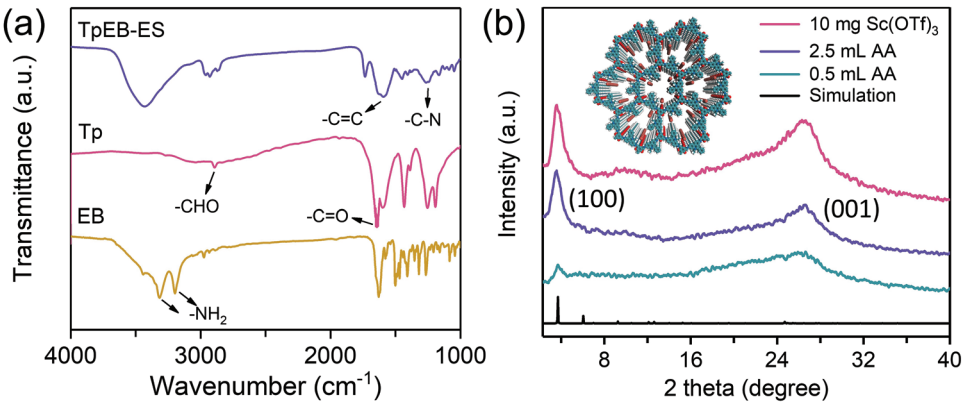

Figure 2. Characterization on the TpEB-ES powder. a) FT-IR spectra of the monomers and TpEB-ES. b) Experimental and simulated XRD patterns of the TpEB-ES powders. Inset in (b) shows the structural model of TpEB.

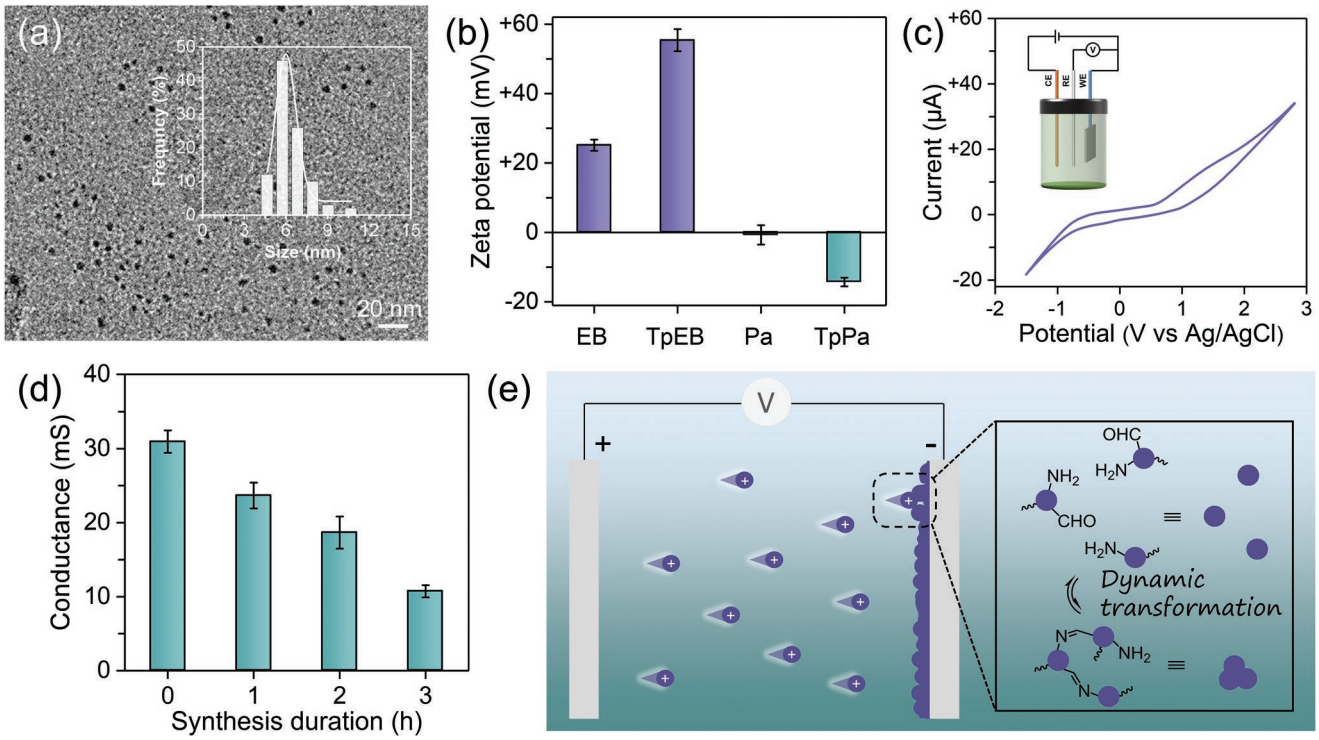

Figure 3. Study on the mechanism of electrosynthesis. a) TEM image and the particle size distribution of the TpEB nuclei. b) Zeta potentials of the monomers and synthesis solutions. c) CV curves of the synthesis solution. d) Conductance of the ITO support after different synthesis durations. e) Schematic illustration of the film formation. Inset in (c) shows the three-electrode system used for the measurements.

fitting based on nonlocal density functional theory (NLDFT) recognizes similar pore size distributions, showing its microporous nature with a pore size of ≈1.8 nm (Figure S3f, Supporting Information). Based on these results, we conclude that TpEB-ES presents the same chemical composition and a similar structure with the solvothermally synthesized counterparts.

2.2. Mechanism Investigation of Electrically Synthesizing TpEB Films

In the light of the accessibility of TpEB films on conductive supports by electrosynthesis, we then seek to explore the underlying mechanism of the film growth. As shown in **Figure 3**a, upon the mixing of monomer solutions, the TpEB crystal nuclei with sizes ranging from ≈5 to ≈10 nm are clearly observed by transmission electron microscopy (TEM) imaging. The rapid generation of such small nuclei rather than large crystals mostly stems from the high activity of Schiff-base reaction under an extraordinarily low monomer concentration (0.18 mmol L^{-1} for Tp in our case). The results of liquid Zeta potential tests verify the positively charged nature of EB molecules (Figure 3b). The cationic monomer consequently endows the resultant COF nuclei with the identical charge property, while the potential is largely increased. Thus, imposing the electric field on the synthesis system leads to the directional migration of cationic TpEB crystal nuclei to the cathode.[18a] To study the reactions in the synthesis, cyclic voltammetry (CV) curves of the monomer solutions and nuclei dispersion were measured using a typical three-electrode system (Figure 3c; Figure S4, Supporting Information). Clearly, no significant oxidative or reductive bands are observed, thus excluding the occurrence of electrode reactions, which are usually involved in conventional electrochemical synthesis. In the film growth, the changes in the conductance of ITO support were recorded in order to reflect the accumulation of TpEB. The results depicted in Figure 3d manifest a gradually decreased trend with extended synthesis duration from 0 to 3 h. This is due to the increasingly integral covering of nonconducting TpEB on ITO supports, thereby diminishing the surface conductivity. In view of this, once a relatively continuous TpEB film is formed, the regional current at the corresponding area declines sharply owning to the impaired conductance. As a result, the charged nuclei as well as EB molecules, will be preferentially deposited on the uncovered blank areas, where a higher current in favor of the TpEB growth exists. The region-selective deposition of TpEB nuclei is helpful to prevent the obtained films from intrinsic defects, suggesting a self-repairing ability in the film formation to ensure its integrity.[30] This inference is further validated by the digital and SEM images of cathode ITO supports after different synthesis durations (Figure S2, Supporting Information). In the final stage of film formation, the continuous but non-conductive TpEB covering is likely to act as an isolating layer to restrain the excessive growth, which results in a self-limiting growth of TpEB films to give reduced thicknesses, analogous to the films prepared by interfacial strategies.[31] According to the above results, we reason that the film formation is likely to be synergistically promoted by the applied electric field and the assembly of nuclei on the support (Figure 3e). On the one hand, the cationic TpEB nuclei coupled with EB molecules directionally migrate to the

cathode in the presence of electric field. It is noteworthy that the electric field also impels the generated TpEB nuclei to form films on the cathode rather than aggregating in the bulk solution (Figures S5 and S6, Supporting Information), showing a high-throughput feature.[32] On the other hand, the reversibility of Schiff-base reaction between Tp and EB enables the crystallization of deposited nuclei,[21] thus producing continuous films without obvious defects or cracks within a short period. Specifically, the well-grown TpEB film can be obtained within 3-h synthesis under an electric field intensity of 50 V cm^{-1}.

Particularly, the viability of electrosynthesis to fabricate ionic COF films lies in the charge property and intensity. Taking TpPa, an extensively studied COF with neutral skeletons (Figure S7, Supporting Information), as an example, we investigated its film formation on ITO supports by the above-suggested electrical strategy. TpPa shows a comparatively weak charge property, displaying a negative Zeta potential of ≈–14 mV (Figure 3b), which agrees well with the previously reported results of the TpPa membranes.[33] According to the macroscopic observation, the light brown covering is generated on the ITO support after 8 h under the electric field intensity of 50 V cm^{-1}; however, the SEM imaging demonstrates that the TpPa layer is composed of loosely stacked nanoparticles (Figure S8, Supporting Information), analogous to the COF films produced by the electrophoresis deposition.[22] In sharp contrast to the dense TpEB films, the perforated structure with undesired mesopores is involved in the TpPa films, suggesting the important role of charge intensity in electrosynthesis. As a matter of fact, the migration velocity of charged nanoparticles under the electric field is positively related to their charge intensity.[18a] When COFs with a high charge intensity are applied, such as cationic TpEB, the preliminary crystal nuclei can be rapidly deposited onto the support to coalesce with each other, thus forming well-integrated continuous films. On the contrary, the migration of COF nuclei with a low charge intensity is significantly hampered. This leads to the aggregation of nuclei in the bulk solution to form large particles instead of directly assembling on the electrode to generate films. We should note that, with a sufficient synthesis duration of as long as 8 h, the TpPa nanoparticles still can be deposited onto the support to produce the structure shown before. Moreover, considering its slightly negative charges, we observe that TpPa grows on the anode exclusively, which is contrary to that of TpEB. The result is a reasonable evidence revealing the crucial influence of charge property on the location of films formed.

2.3. Membrane Preparation and Characterization

Having proved the electrosynthesis feasible, we subsequently studied its viability of producing TpEB membranes for separation applications. As for nanofiltration, membrane materials featuring both ordered and charged pores are highly desirable for performance improvement.[34] Hence, ionic COFs could be one of the ideal building materials for high-quality nanofiltration membranes. Unfortunately, separation membranes based on ionic COFs are largely unexplored.[29] In our study, the Au-coated anodic aluminum oxide (AAO) support with a nominal pore size of 100 nm is chosen as the porous substrate to grow cationic TpEB membranes. The Au plating dramatically enhances the conductance of the AAO supports, without damaging their porous structures (**Figure 4**a; Figures S9 and

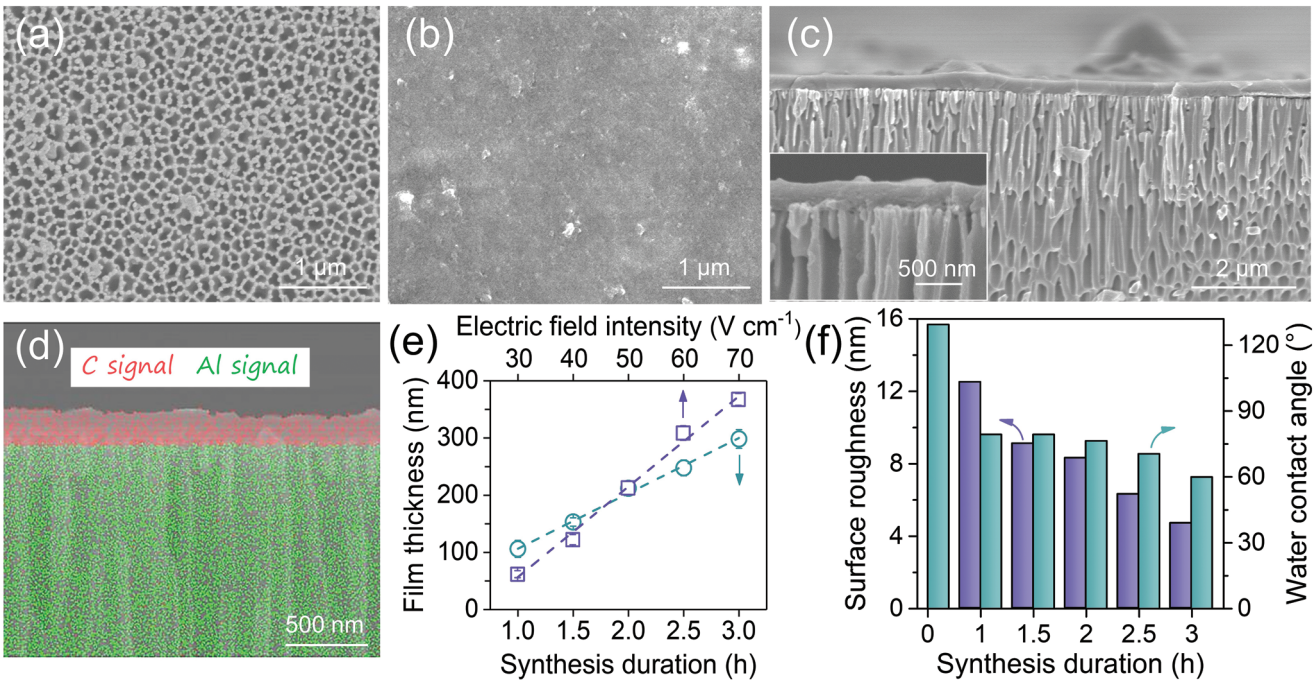

Figure 4. Characterization on the electrically synthesized TpEB membranes. a) Surface SEM image of the Au-coated AAO support. b) Surface and c) cross-sectional SEM images of the TpEB membrane. d) Cross-sectional EDX mapping of the TpEB membrane. e) Thickness of the TpEB layer versus the synthesis duration and electric field intensity. f) Surface roughness and WCA of the membranes. Inset in (c) is a magnified SEM image. Images shown in (b–d) correspond to the membrane synthesized at 50 V cm^{-1} for 2 h.

S10, Supporting Information). We then electrically synthesized TpEB layers under the catalysis of AA on Au-coated AAO supports to produce composite membranes. To this end, the Au-coated AAO support was tightly attached to the bottom of the conductive side of cathode ITO, while the neat ITO acted as the anode. After 3 h of electrosynthesis, the original dark gray Au-coated AAO support appears a light brown color (Figure S11, Supporting Information), implying the membrane formation. The successful preparation of TpEB layers on AAO supports was further confirmed by FT-IR, XRD, and X-ray photoelectron spectroscopy (XPS) characterizations (Figure S12, Supporting Information). To be specific, the FT-IR and XRD results of TpEB membranes correspond with the TpEB powders. Moreover, XPS detects the Br element on membrane surface, further proving the generation of TpEB.

To study the growth and crystallization of TpEB on the Au-coated AAO substrate, we examined the time-dependent SEM images after different synthesis durations within 1 h under 50 V cm^{-1}. As shown in Figure S13 (Supporting Information), a 10-min synthesis enables the deposition of TpEB crystal nuclei along with the skeleton of AAO pore walls. Subsequently, the nuclei combine with their neighbors to form sheet-like coverings. With the region-selective deposition, the majority of AAO supports can be covered with TpEB at 40 min, and a continuous selective layer is then generated at 1 h (Figure S14a, Supporting Information). Next, we studied the morphology of TpEB membranes synthesized for 1–3 h. Compared with the large-pore Au-coated AAO support, the well-grown TpEB layer in the absence of any defects, cracks, or pinholes is observed on the top surface after a 2 h synthesis under the electric field intensity of 50 V cm^{-1} (Figure 4b). Remarkably, the duration required to produce complete COF membranes via electrosynthesis is much shorter than most of other reported methods (Table S1, Supporting Information), indicating the high productivity of our strategy. The cross-sectional SEM image reveals a continuous TpEB separation layer with a uniform thickness (Figure 4c). From the magnified SEM observation, it is clear that the TpEB layer with a thickness of ≈210 nm attaches well to the support without noticeable gaps (inset in Figure 4c). The energy-dispersive X-ray spectroscopy (EDX) analysis substantially validates a sharp transition between TpEB layer (C signals) and AAO support (Al signals; Figure 4d), implying negligible nucleation and growth of TpEB in the AAO pores. Significantly, the structure of the obtained TpEB layers, especially the thickness, can be readily tuned by varying the electric field intensity and synthesis duration (Figure S14–S17 in Supporting Information). In detail, the TpEB thickness presents a nearly linear correlation with the above two parameters, which is adjustable in the range of ≈50–400 nm (Figure 4e). Atomic force microscopy characterizations were performed to gain insights into the topographic features of the fabricated membranes. Figure 4f and Figure S18 (Supporting Information) depict an incessantly decreased roughness with prolonged synthesis durations. We attribute the roughness decrease to the preferred growth of TpEB at the shallow areas through the electrically enabled selective growth, thereby equilibrating the geology to produce a smoothed surface.[35] Additionally, the formation of TpEB on Au-coated AAO supports gives rise to a promotional hydrophilicity with significantly reduced water contact angles (WCAs) from ≈120° to ≈60° (Figure 4f; Figure S19, Supporting Information), benefiting the cross-membrane water permeation. In addition to the inorganic supports (i.e., ITO, and AAO), TpEB layers are also electrically available on Au-coated polysulfone membranes (Figure S20, Supporting Information). The results evidently prove the general applicability of the electrosynthesis protocol in constructing ionic COF selective layers on various conductive supports.

2.4. Molecular Separation Performances of TpEB Membranes

To evaluate the detailed membrane performance, we quantified the pure water permeances and molecular rejection rates of the membranes produced under various synthetic conditions with AA as catalyst. It should be noted that the Au-coated AAO support presents a water permeance of ≈4000 L m^{-2} h^{-1} bar^{-1}, and its Congo red (CR) and acid fuchsin (AF) rejection rates are both below 10%. **Figure 5**a illustrates the permselectivity of the membranes obtained under diverse electric field intensities with a constant synthesis duration of 2 h. We can observe that the water permeance sharply decreases with the intensification of the applied electric field. This is in good agreement with the raised thickness of TpEB layers (Figure 4e; Figure S17, Supporting Information), which reduces the permeance because of raised mass transfer resistance.[36] Significantly, the TpEB membrane produced under 50 V cm^{-1} realizes 93.3% rejection of CR molecules, with a high water permeance of 344.6 L m^{-2} h^{-1} bar^{-1}, which shows the optimal permselectivity. Then, the membrane performance against the synthesis durations was investigated at this electric field intensity (Figure 5b). Within short synthesis durations, the resulting membranes constantly give high water permeances and decent CR rejection rates. For instance, a synthesis duration of merely 1 h endows the membrane with an ultrahigh permeance of 1526 L m^{-2} h^{-1} bar^{-1} and a CR rejection of 81%. The prolongation of synthesis duration slightly improves the rejection rates accompanied by largely reduced water permeances. In the case of AF, the rejection rates follow a continuous increase tendency, and a notable removal efficiency of over 99% is attained with 3 h synthesis. This membrane selectivity can be adequately sustained for at least six cycles (Figure S21, Supporting Information). Inspired by the high crystallinity using $Sc(OTf)_3$, we prepared TpEB membranes by following this catalysis condition. The $Sc(OTf)_3$-catalyzed membranes exhibit similar morphologies to those generated by AA (Figure S22, Supporting Information). As intended, these membranes show increased permeances with comparable CR rejections (Figure S23, Supporting Information), suggesting the positive correlation between COF crystallinity and membrane performance. Consistent with the tunable thickness, the electrically synthesized TpEB membranes demonstrate an adjustable permselectivity, exhibiting pronounced water permeances that surpass the majority of the previously reported COF membranes (Table S2). These results demonstrate the advantage of change-enhanced molecular separation, which mostly originates from the relatively ordered and charged nanochannels of cationic TpEB. In these filtration results, of particular interest is that the distinct selectivity difference between CR and AF can be visualized for the membrane produced at a short duration of 1 h. This could be attributed to the size and charge

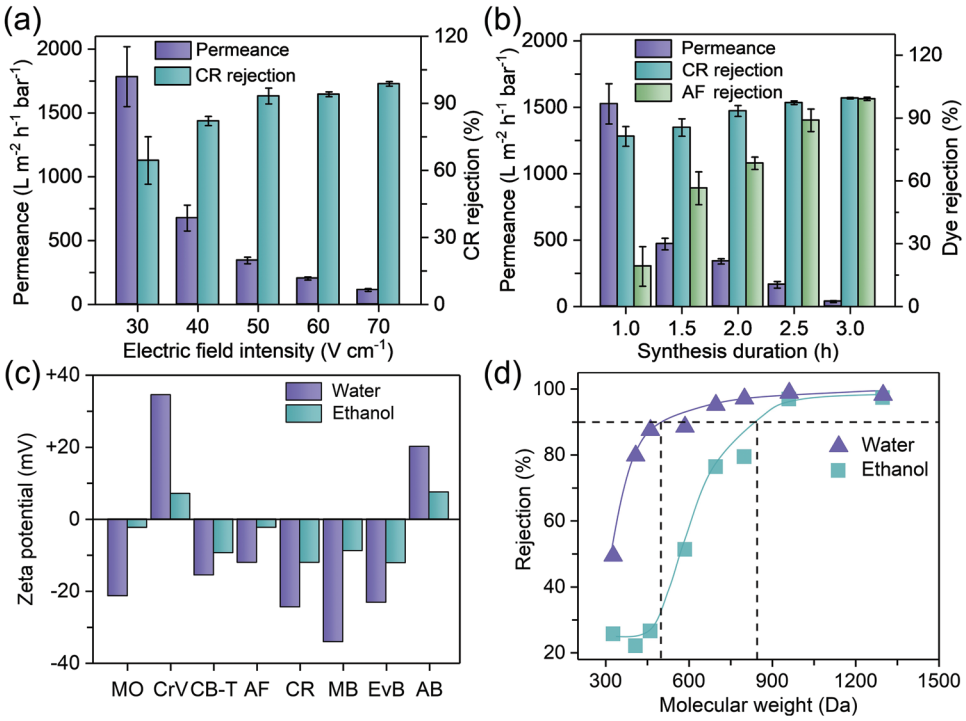

Figure 5. Separation performance of the TpEB membranes with AA as catalyst. Water permeance and dye rejection of the membranes prepared with varied a) electric field intensities and b) synthesis durations. c) Zeta potentials of dyes dissolved in water and ethanol. d) Rejection rates to dyes dissolved in water and ethanol.

diversity of the adopted probe molecules. The top TpEB selective layers exhibit a pore size of ≈1.8 nm, which is smaller than CR (2.6×0.7 nm^2) and larger than AF (1.2×1.1 nm^2). Hence, it is rationalized that the membrane is competent to reject CR molecules while allowing the pass of AF molecules. Meanwhile, the positively charged pores create the capture of negatively charged CR and AF molecules through electrostatic attractions at the early stage of filtration, thus reducing the effective sieving size.[37] This kind of masking effect is much more pronounced for CR molecules due to their larger size and higher charge intensity (Figure 5c), thus leading to the enhanced selectivity.

To profoundly study the charge-enhanced separation, we evaluated the interception ability of our membranes using a range of anionic and cationic dyes dissolved in water and ethanol (Figure S24, Supporting Information). Here, ethanol essentially weakens the charge properties of dyes, as validated by distinctly reduced Zeta potential values (Figure 5c), which will in return compromise the electrostatic interaction between charged molecules and TpEB channels during filtration. Consequently, the selectivity for dyes with molecular weights below 800 Da is degraded in ethanol compared with that in water (Figure 5d; Figure S25 and S26, Supporting Information). This selectivity degradation is particularly noticeable for molecules like methyl orange (MO) and crystal violet (CrV), mainly due to their small sizes combined with significantly compromised charge interactions. The above results reasonably illustrate the charge-dominated separation of charged molecules.[38] In addition, the TpEB membrane preserves high rejections to molecules with molecular weights >900 Da in ethanol, indicating the contribution of size-based exclusion to separation performances. Therefore, based on the above discussion, we conclude that the excellent nanofiltration performance of TpEB membranes is synergistically dominated by sizes and charges.[39] The result further highlights the unique superiority of ionic COF membranes in liquid molecular separations.

2.5. Charge-Selective Molecular Sieving of TpEB Membranes

The separation and recycling of valuable targets from liquid mixtures of charged and neutral molecules are challenging for traditional nanofiltration membranes.[40] With the capability of charge-dominated molecular separation, our TpEB membranes are expected to implement the precise sieving of charged and neutral molecules with similar sizes and molecular weights (**Figure 6**a). To substantiate this, we conducted the separation of charge-free vitamin B12 (VB-12), a biomolecule vital for the production of bone marrow erythrocytes, from the mixture containing anionic chrome black T (CB-T) or cationic Alcian blue 8GX (AB) (Figure 6b). VB-12 presents a molecular weight of 1355 Da, which is close to that of AB (1299 Da). In spite of its large molecular weight, VB-12 presents a spherical structure with a fine size of 1.7×1.8 nm^2, similar to the lateral size of CB-T (1.6 nm). As shown in Figure 6c, a dark blue mixture derived from cyan AB solution and light pink VB-12 solution was filtrated by the TpEB membrane, which results in a pink filtrate with the identical color of VB-12, suggesting the discrimination of the molecule pairs. The precise sieving ability is further confirmed by the UV–vis spectra (Figure 6d). The spectrum of the

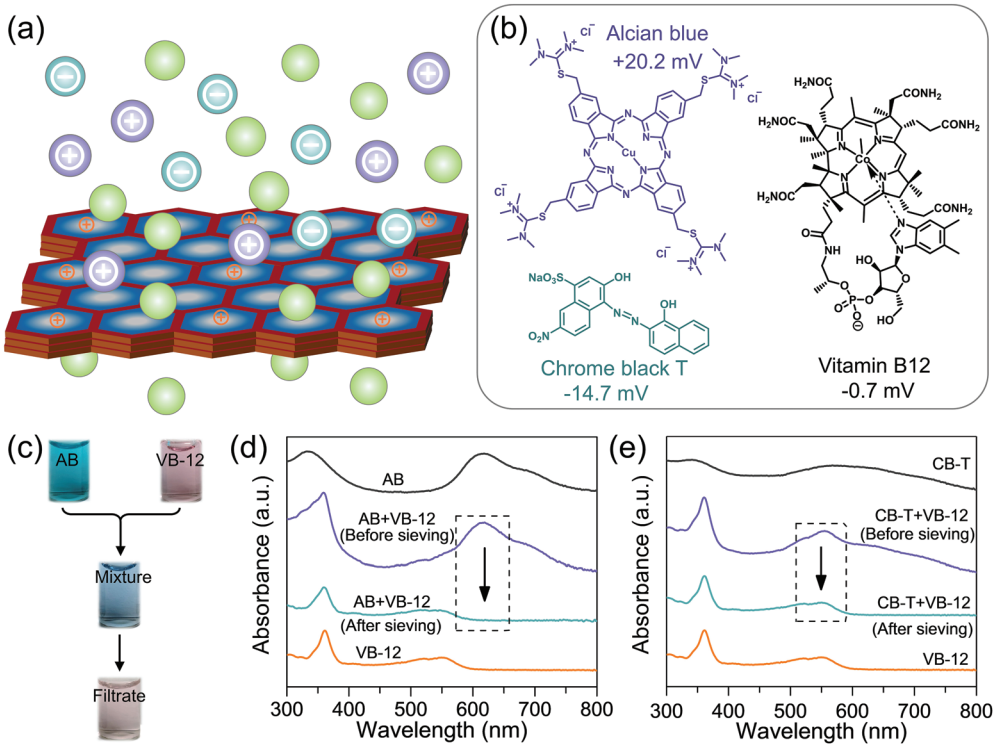

Figure 6. Charge-selective molecular sieving of the TpEB membrane. a) Schematic illustration of the sieving between charged and neutral molecules. b) Molecular structures of CB-T, VB-12, and AB. c) Photographs of the charge-selective separation of AB/VB-12. UV-vis spectra of the sieving of d) AB/VB-12 and e) CB-T/VB-12. The membrane was synthesized at 50 V cm^{-1} for 2 h with AA as catalyst.

filtrate primarily overlaps with that of the pure VB-12 solution, and the characteristic peak of AB at ≈620 nm disappears, while preserving the characteristic peak of VB-12 at ≈360 nm, which suggests a 98% rejection of AB with a negligible retention of VB-12 (≈2%). The charge selectivity is also applicable for separating negatively charged CB-T from the mixture, as depicted in Figure 6e and Figure S27 (Supporting Information). Results of these explicitly reveal the charge-selective molecular sieving of the TpEB membrane. In other words, charged molecules can be effectively rejected through the electrostatic interaction and pore sieving, while the neutral molecules receive a free traverse across the membrane. We anticipate that the charge-selective nanochannels offered by cationic COFs are highly attractive for practical applications.

3. Conclusion

In summary, we have developed a highly efficient electrosynthesis protocol enabling the fast preparation of ionic COF membranes for charge-selective nanofiltration. The intrinsic charge property and intensity of ionic TpEB are of great importance for electrically generating well-integrated films. By designing conductive porous supports, the suggested electrical strategy further realizes the generation of TpEB membranes within a short duration of 3 h, largely improving the productivity of COF membranes. The growth and thus the performance of cationic TpEB membranes can be precisely regulated by altering the electrical conditions. The optimized membrane provides a high separation ability with pronounced water permeances that exceed the majority of COF nanofiltration membranes. We have demonstrated that the prominent performance arises from the relatively uniform aperture sizes as well as the synergistic contribution of charge- and size-based exclusion. The distinctive charge-selective feature is surprisingly observed in the cationic nanochannels of TpEB membranes, achieving the efficient sieving of charged and neutral molecules. This study of electrically synthesizing ionic COF membranes provides a new avenue for engineering advanced membranes with functionalized nanochannels to tackle challenging separations.

Supporting Information

Supporting Information is available from the Wiley Online Library or from the author.

Acknowledgements

This work was supported by the National Natural Science Foundation of China (22008110, 21825803). The authors also thank the Project of Priority Academic Program Development of Jiangsu Higher Education Institutions (PAPD) and the China Postdoctoral Science Foundation (2020M681568) for support.

Conflict of Interest

The authors declare no conflict of interest.

Data Availability Statement

The data that support the findings of this study are available in the supplementary material of this article.

Keywords

charge selectivity, electrosynthesis, ionic covalent organic frameworks, molecular separation, nanochannels

Received: November 16, 2021
Revised: January 20, 2022
Published online: February 26, 2022

[1] A. P. Cote, A. I. Benin, N. W. Ockwig, M. O'Keeffe, A. J. Matzger, O. M. Yaghi, *Science* **2005**, *310*, 1166.
[2] a) Z. C. Guo, Z. Q. Shi, X. Y. Wang, Z. F. Li, G. Li, *Coord. Chem. Rev.* **2020**, *422*, 213465; b) X. Zhao, P. Pachfule, A. Thomas, *Chem. Soc. Rev.* **2021**, *50*, 6871; c) H. S. Sasmal, S. Bag, B. Chandra, P. Majumder, H. Kuiry, S. Karak, S. Sen Gupta, R. Banerjee, *J. Am. Chem. Soc.* **2021**, *143*, 8426; d) A. K. Mohammed, S. Usgaonkar, F. Kanheerampockil, S. Karak, A. Halder, M. Tharkar, M. Addicoat, T. G. Ajithkumar, R. Banerjee, *J. Am. Chem. Soc.* **2020**, *142*, 8252.
[3] S. Yuan, X. Li, J. Zhu, G. Zhang, P. Van Puyvelde, B. Van der Bruggen, *Chem. Soc. Rev.* **2019**, *48*, 2665.
[4] a) K. Dey, M. Pal, K. C. Rout, H. S. Kunjattu, A. Das, R. Mukherjee, U. K. Kharul, R. Banerjee, *J. Am. Chem. Soc.* **2017**, *139*, 13083; b) H. S. Sasmal, A. Halder, H. S. Kunjattu, K. Dey, A. Nadol, T. G. Ajithkumar, P. Ravindra Bedadur, R. Banerjee, *J. Am. Chem. Soc.* **2019**, *141*, 20371; c) K. Dey, S. Bhunia, H. S. Sasmal, C. M. Reddy, R. Banerjee, *J. Am. Chem. Soc.* **2021**, *143*, 955.
[5] a) H. Fan, A. Mundstock, A. Feldhoff, A. Knebel, J. Gu, H. Meng, J. Caro, *J. Am. Chem. Soc.* **2018**, *140*, 10094; b) X. Shi, Z. Zhang, S. Fang, J. Wang, Y. Zhang, Y. Wang, *Nano Lett.* **2021**, *21*, 8355.
[6] C. Yin, Z. Zhang, J. Zhou, Y. Wang, *ACS Appl. Mater. Interfaces* **2020**, *12*, 18944.
[7] Z. Wang, S. Zhang, Y. Chen, Z. Zhang, S. Ma, *Chem. Soc. Rev.* **2020**, *49*, 708.
[8] C. Zhang, Y. Li, H. Li, Q. Zhang, J. Lu, *J. Mater. Chem. C* **2021**, *9*, 374.
[9] X. Zhang, K. Wan, P. Subramanian, M. Xu, J. Luo, J. Fransaer, *J. Mater. Chem. A* **2020**, *8*, 7569.
[10] C. Gu, Y. Chen, Z. Zhang, S. Xue, S. Sun, K. Zhang, C. Zhong, H. Zhang, Y. Pan, Y. Lv, Y. Yang, F. Li, S. Zhang, F. Huang, Y. Ma, *Adv. Mater.* **2013**, *25*, 3443.
[11] a) Y. Zhao, Y. Wei, L. Lyu, Q. Hou, J. Caro, H. Wang, *J. Am. Chem. Soc.* **2020**, *142*, 20915; b) Y. Liu, Y. Wei, M. Liu, Y. Bai, X. Wang, S. Shang, J. Chen, Y. Liu, *Angew. Chem., Int. Ed.* **2021**, *60*, 2887.
[12] a) C. Gu, N. Huang, J. Gao, F. Xu, Y. Xu, D. Jiang, *Angew. Chem., Int. Ed.* **2014**, *53*, 4850; b) X. He, H. Sin, B. Liang, Z. A. Ghazi, A. M. Khattak, N. A. Khan, H. R. Alanagh, L. Li, X. Lu, Z. Tang, *Adv. Funct. Mater.* **2019**, *29*, 1900134.
[13] J. F. Feng, T. F. Liu, R. Cao, *Angew. Chem., Int. Ed.* **2020**, *59*, 22392.
[14] C. Zeng, B. Wang, H. Zhang, M. Sun, L. Huang, Y. Gu, Z. Qiu, K. Mullen, C. Gu, Y. Ma, *J. Am. Chem. Soc.* **2021**, *143*, 2682.
[15] H. Zhang, Y. Zhang, C. Gu, Y. Ma, *Adv. Energy Mater.* **2015**, *5*, 1402175.
[16] a) Z. Zhou, D. Guo, D. B. Shinde, L. Cao, Z. Li, X. Li, D. Lu, Z. Lai, *ACS Nano* **2021**, *15*, 11970; b) Z. Zhou, X. Li, D. Guo, D. B. Shinde, D. Lu, L. Chen, X. Liu, L. Cao, A. M. Aboalsaud, Y. Hu, Z. Lai, *Nat. Commun.* **2020**, *11*, 5323.
[17] S. Zhou, Y. Wei, L. Li, Y. Duan, Q. Hou, L. Zhang, L. X. Ding, J. Xue, H. Wang, J. Caro, *Sci. Adv.* **2018**, *4*, eaau1393.
[18] a) L. Besra, M. Liu, *Prog. Mater Sci.* **2007**, *52*, 1; b) X. Zhang, Y. Li, C. Van Goethem, K. Wan, W. Zhang, J. Luo, I. F. J. Vankelecom, J. Fransaer, *Matter* **2019**, *1*, 1285.
[19] G. He, M. Dakhchoune, J. Zhao, S. Huang, K. V. Agrawal, *Adv. Funct. Mater.* **2018**, *28*, 1707427.
[20] a) H. Ma, Y. Chen, X. Li, B. Li, *Adv. Funct. Mater.* **2021**, *31*, 2101861; b) J. M. Lee, A. I. Cooper, *Chem. Rev.* **2020**, *120*, 2171.
[21] J. L. Segura, M. J. Mancheno, F. Zamora, *Chem. Soc. Rev.* **2016**, *45*, 5635.
[22] J. M. Rotter, S. Weinberger, J. Kampmann, T. Sick, M. Shalom, T. Bein, D. D. Medina, *Chem. Mater.* **2019**, *31*, 10008.
[23] a) Y. Peng, Z. Hu, Y. Gao, D. Yuan, Z. Kang, Y. Qian, N. Yan, D. Zhao, *ChemSusChem* **2015**, *8*, 3208; b) N. Huang, P. Wang, M. A. Addicoat, T. Heine, D. Jiang, *Angew Chem Int Ed Engl* **2017**, *56*, 4982; c) S. Mitra, S. Kandambeth, B. P. Biswal, M. A. Khayum, C. K. Choudhury, M. Mehta, G. Kaur, S. Banerjee, A. Prabhune, S. Verma, S. Roy, U. K. Kharul, R. Banerjee, *J. Am. Chem. Soc.* **2016**, *138*, 2823; d) L. Wang, C. Zeng, H. Xu, P. Yin, D. Chen, J. Deng, M. Li, N. Zheng, C. Gu, Y. Ma, *Chem. Sci.* **2019**, *10*, 1023.
[24] C. Yin, S. Fang, X. Shi, Z. Zhang, Y. Wang, *J. Membr. Sci.* **2021**, 618.
[25] C. H. Yang, J. S. Chang, D. J. Lee, *Chemosphere* **2020**, *253*, 126736.
[26] Y. Ying, M. Tong, S. Ning, S. K. Ravi, S. B. Peh, S. C. Tan, S. J. Pennycook, D. Zhao, *J. Am. Chem. Soc.* **2020**, *142*, 4472.
[27] H. Ma, B. Liu, B. Li, L. Zhang, Y. G. Li, H. Q. Tan, H. Y. Zang, G. Zhu, *J. Am. Chem. Soc.* **2016**, *138*, 5897.
[28] M. Matsumoto, R. R. Dasari, W. Ji, C. H. Feriante, T. C. Parker, S. R. Marder, W. R. Dichtel, *J. Am. Chem. Soc.* **2017**, *139*, 4999.
[29] P. Zhang, Z. Wang, P. Cheng, Y. Chen, Z. Zhang, *Coord. Chem. Rev.* **2021**, 438.
[30] R. Wei, H. Y. Chi, X. Li, D. Lu, Y. Wan, C. W. Yang, Z. Lai, *Adv. Funct. Mater.* **2019**, *30*, 1907089.
[31] Q. Hao, C. Zhao, B. Sun, C. Lu, J. Liu, M. Liu, L. J. Wan, D. Wang, *J. Am. Chem. Soc.* **2018**, *140*, 12152.
[32] C. Gu, N. Huang, Y. Chen, L. Qin, H. Xu, S. Zhang, F. Li, Y. Ma, D. Jiang, *Angew. Chem., Int. Ed.* **2015**, *54*, 13594.
[33] X. Shi, R. Wang, A. Xiao, T. Jia, S.-P. Sun, Y. Wang, *ACS Appl. Nano Mater.* **2018**, *1*, 6320.
[34] a) H. Yang, L. Yang, H. Wang, Z. Xu, Y. Zhao, Y. Luo, N. Nasir, Y. Song, H. Wu, F. Pan, Z. Jiang, *Nat. Commun.* **2019**, *10*, 2101; b) J. Shen, R. Zhang, Y. Su, B. Shi, X. You, W. Guo, Y. Ma, J. Yuan, F. Wang, Z. Jiang, *J. Mater. Chem. A* **2019**, *7*, 18063.
[35] L. Sheng, C. Wang, F. Yang, L. Xiang, X. Huang, J. Yu, L. Zhang, Y. Pan, Y. Li, *Chem. Commun.* **2017**, *53*, 7760.
[36] A. Xiao, X. Shi, Z. Zhang, C. Yin, S. Xiong, Y. Wang, *J. Membr. Sci.* **2021**, 624.
[37] a) W. Zhang, L. Zhang, H. Zhao, B. Li, H. Ma, *J. Mater. Chem. A* **2018**, *6*, 13331; b) T. Chen, B. Li, W. Huang, C. Lin, G. Li, H. Ren, Y. Wu, S. Chen, W. Zhang, H. Ma, *Sep. Purif. Technol.* **2021**, *256*, 117787.
[38] a) Z. Zhang, X. Xiao, Y. Zhou, L. Huang, Y. Wang, Q. Rong, Z. Han, H. Qu, Z. Zhu, S. Xu, J. Tang, J. Chen, *ACS Nano* **2021**, *15*, 13178; b) Z. Zhang, M. M. Rahman, C. Abetz, A. L. Hohme, E. Sperling, V. Abetz, *Adv. Mater.* **2020**, *32*, 1907014.
[39] M. Hu, S. Yang, X. Liu, R. Tao, Z. Cui, C. Matindi, W. Shi, R. Chu, X. Ma, K. Fang, M. Titus, B. B. Mamba, J. Li, *Sep. Purif. Technol.* **2021**, *266*, 118587.
[40] N. S. Naik, M. Padaki, A. M. Isloor, K. K. Nagaraja, K. A. Vishnumurthy, *Chem. Eng. J.* **2021**, *418*, 129372.